Stellar Spectra A. Basic Line Formation

Andreas Ellewsen[1]

[1] Institute of theoretical astrophysics

1. Introduction

This is the first of three numerical exercises in the course on Radiative processes in astrophysics (AST4310) at the University of Oslo. In this exercise we are to follow the steps of Annie Cannon, Cecilia Payne, and Marcel Minnaert. By doing this we hope to learn about the use of spectral lines in astophysics. I will be using cgs units for all calculations in this project.

2. Spectral Classification

The first part of this section deals with learning a little about how IDL functions. You also make a fuction that adds all the numbers in an array together and gives you the result. This function already exists in IDL, and is called TOTAL, but we make our own function anyway. The function is called ADDUP, and looks exactly like the function written in the exercise text. The function has been tested, and it passes all the test I've tried throwing at it (except of course those it will clearly fail, like strings). Note however that I will not be using IDL for this project since I know python better than IDL.

The second part of this section deals with LaTeX and gives instructions on how to write a good report. Basically one is given a template and told a long list of things that are useful to know when writing reports, and then you use this knowledge for the rest of the exercise.

3. Saha-Boltzmann calibration of the Harvard sequence

Here we want to explain the spectral-type sequence that was studied in the two first parts of the last section (which we ignored). To start of we study figures 5 and 7 in the exercise text. Starting from the right of figure 5 one sees that the $H\beta$ line lies between 4762Å and 4954Å. If one looks at figure 7 one sees that the only line between these two wavelengths is the Balmer β line at 4861Å. The Balmer β line is the transition between $n = 4$ and $n = 2$. Considering that the spectrum we're looking at in figure 5 ranges between 3900Å and 5000Å, which is in the visual part of the spectrum, the rest of the lines corresponding to hydrogen should all be in the Balmer series as well. This means that none of the lines share the same upper level, and that they all share the same lower level, namely $n = 2$. This is the case for all of these named series. Sharing of the upper levels is a bit more complicated. If one looks at figure 7 one sees that Lyman α shares no upper level with anything. But Lyman β shares the same upper level as Balmer α. Figure 7 skips some of the transitions. But Lyman γ shares upper level with Balmer β and Paschen α. It keeps going in this way for the rest of the transitions.

At this point Payne made the assumption that the strength of the absorption lines observed in stellar spectra scaled with the population density of the lower level of the corresponding transition. Assuming that most of the hydrogen is in the lower energy levels it is logical that most of the transitions must be going upwards in the levels, and thus they should scale with the population density of the lower levels. It turns out that this assumption assumption is not correct, but in general it is true that stellar absorption lines get stronger at larger lower-level population. We ignore this and continue with Payne's assumption anyway.

If we assume that the above is true. We can give som rough estimates of the strength ratios of the α lines in the HI Lyman, Balmer, Paschen and Brackett series. We see from figure 7 in the exercise that Lyman α releases about $10eV$, while Balmer releases about $2eV$, Paschen $0.5eV$ and Brackett about $0.25eV$. Considering that our assumption means more transitions from lower levels, the Lyman α line should be much stronger than the Balmer. And the Balmer should be much stronger than the Paschen and so forth.

Next we need to define some functions:

The Boltzmann distribution is defined

$$\frac{n_{r,s}}{N_r} = \frac{g_{r,s}}{U_r} e^{-\chi_{r,s}/kT} \tag{1}$$

The Partition function U_r is defined as

$$U_r = \sum_s g_{r,s} e^{-\chi_{r,s}/kT} \tag{2}$$

The Saha law reads

$$\frac{N_{r+1}}{N_r} = \frac{1}{N_e} \frac{2U_{r+1}}{U_r} \left(\frac{2\pi m_e kT}{h^2} \right)^{3/2} e^{-\chi_r/kT}. \tag{3}$$

We will use this to study a fictional element known as Schadeenium(E). Schadeenium has

- ionization energies $\chi_1 = 7$ eV for neutral E, $\chi_2 = 16$eV for E^+, $\chi_3 = 31$eV for E^2+, $\chi_4 = 51$eV for E^3+.
- excitation energies that increase incrementally by 1 eV: $\chi_{r,s} \equiv s - 1$ eV in each stage
- statistical weights $g_{r,s} \equiv 1$ for all levels (r,s)

Table 1 on page 12 of the exercise shows different values of the 3 functions for our element. When looking at this it is clear that the partition function is weakly dependent on temperature. In the table with calulcations for the boltzmann function we see a steep decline in the population for higher levels. The higher levels do fill up if one raises the temperature but the ground state always has the largest population. From this it is clear that the lower levels are the most important ones. For real atoms the energy difference between levels 1 and 2 are usually larger than for E, and thus their partition functions are often well approixmated by the statistical weight of the ground state.

The reason for the difference in behaviour between the Saha and Boltzmann distributions is caused by the $(...)^{3/2}$ factor in front of the exponential in the Saha distribution. The Boltzmann distribution doesn't have this factor and thus it converges towards $g_{r,s}/U_r$ for hight T while Saha just keeps rising indefinitely.

Raising the temperature thus causes the distribution between the energy levels to spread out, and even if we don't get a lot of electrons in the higher energy levels, the thermal energy is high enough to cause ionization from the lower levels to the next ionization stage.

Thus we've found that when a gas is in thermal equilibrium we expect to find at most two ionization stages present. And for each ionization there is a steep decline in the population for each energy level.

With this in mind we compute the partition function U_r for Schadeenium and print the values for levels $r = [0, 3]$.

```
[ 1.10887478  1.10887488  1.10887488  1.10887488]
[ 1.45590319  1.45633511  1.45633513  1.45633513]
[ 2.23243073  2.27133987  2.27155094  2.27155097]
```

Which is a perfect match to the values tabulated in the exercise text. We then make a Boltzmann function in the program and check that it functions properly by printing the relative level population for $s = [0, 10]$ for $T = 5000, 10000, 20000$. I'll spare you the wall of text, and just state that the output from the program matches the values given in the exercise text. The next step is to make a Saha function and test that for $r = [1, 6]$ for $T = 20000$ and $P_e = 100$, and for $r = [1, 6]$, with $T = 10000$ and $P_e = 100$. We print the results and get

```
 2.72775113242e-10
0.000180278462885
0.632005363273
0.36781263824
1.71975186581e-06
----
0.000477757567228
0.94509484422
0.0544273981268
8.63969442555e-11
1.56819249959e-29
```

which matches the values given in the exercise, cofirming that the function works as it should. (Note here that the code example in the exercise tells us to calculate the values for an electron pressure that is different from the one used in the table, so I've chosen to use the one corresponding to the table).

3.1. Payne curves for Schadeenium

If TE holds in a stellar atmosphere one may expect that the observed strength of a spectral line involving level (r, s) scales with the Saha-Boltzmann prediction for the lower level population $n_{r,s}$ — even if one doesn't know how spectral lines are formed in detail. That was the underlying premise of Payne's analysis. We follow it by plotting curves for various levels of the neutral and ionization stages of element E. To do this I write a function Sahabolt_E that evaluates $n_{r,s}/N$ for any level of E as a function of T and P_e. Using the same value for electron pressure as before we inspect a few values. I check four different settings.

- $T = 5000$,$P_e = 1000$, $r = 1$, $s = [1, 5]$
- $T = 20000$,$P_e = 1000$, $r = 1$, $s = [1, 5]$

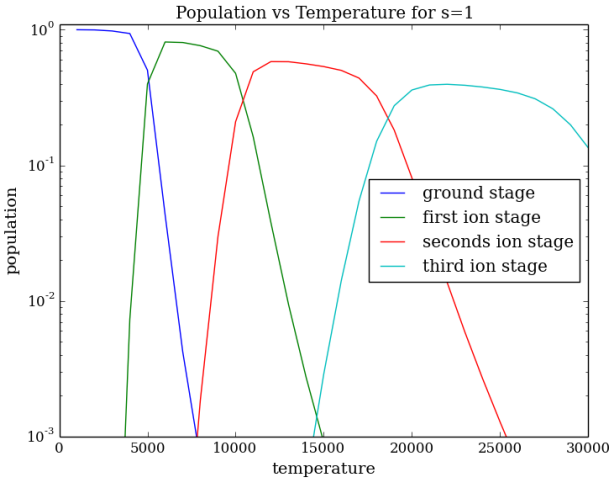

Fig. 1. Population as a function of temperature for $s = 1$.

- $T = 10000$,$P_e = 1000$, $r = 2$, $s = [1, 5]$
- $T = 20000$,$P_e = 1000$, $r = 4$, $s = [1, 5]$

I'll spare you the wall of text this time as well, and just state that the output from the program matches the values given in the exercise text, and confirms what we've already seen; that the lower levels within an ionization stage always have higher population due to the Boltzmann factor. Note also that the drop-off with s is less steep at higher temperature as it should be due to the Saha factor.

Now we have all the tools nescessary to compute the ground-state populations $n_{r,1}/N$ for Payne's pressure ($P_e = 131$ dyne cm^{-}2) and a range of temperatures for each ion r,and plot them together in a Payne-like graph. The resulting plot from this can be seen in figure 1. We see in the plot that the flanks on each side of the peaks is very steep. Mathematically this can be explained by the exponential terms in the product of the Saha and Boltzmann distributions. Physically one could argue that the uncertainty principle is at play here, so that even if the temperature isn't quite high enough to excite the electrons they still get excited to the next level. This way we get a steep but still gradual excitation to the next energy level instead of a straight cut off. Note that if the temperature goes to 0 the electrons would go to the ground stage, and if the temperature goes to infinity all the electrons would leave the ground stage. If ones looks closely one can see that the right side of the curves is less steep than the left side. The explanation for this can be found in the $(...)^{3/2}$ factor in the Saha distribution. Basically this term is fighting the exponentials.

Figures for higher levels of s can be seen in figures 2 & 3.

The change between the three figures is clear straight away. When looking at the ground state for the energy levels we see that the higher the temperature is, the lower the population gets. Studying the plots for higher energy levels we also see that the population moves to higher energy levels for higher ionization levels. If one considers elements with lower ionization energies than E the curves should move towards the right, and become broader. This should become clear by considering the fact that with ionization energies, one would need lower thermal energy to ionize atoms. The edges should be sharper as well, since the fluctuations due to the uncertainty principle can have a bigger impact. Considering higher ionization energies gives us the opposite case with broader curves moved towards the left and becoming narrower.

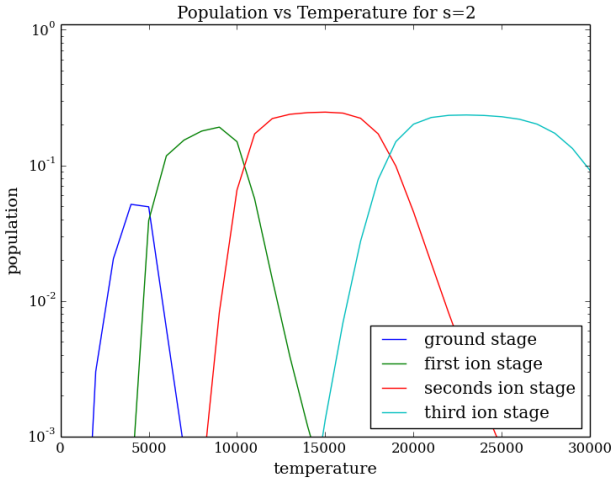

Fig. 2. Population as a function of temperature for $s = 4$.

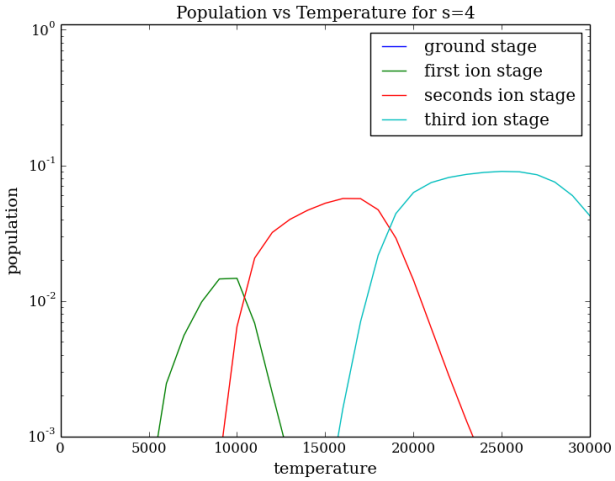

Fig. 3. Population as a function of temperature for $s = 4$.

3.2. Saha-Boltzmann population of hydrogen

Since we've made function for our fictional element it should be easy to transfer this to a real element, namely Hydrogen. To write the functions for Hydrogen we need to know a few things about it first. Hydrogen has ionization energy $\chi_1 = 13.598$ eV. The statistical weight $g_{r,s}$ and level energies $\chi_{r,s}$ of neutral hydrogen are given by

$$g_{1,s} = 2s^2 \ , \ \chi_{1,s} = 13.598(1 - 1/s^2) \text{ eV}$$

while the single ion stage(protons only) has $U_2 = g_{2,1} = 1$. Implementing this worked nicely and i was able to reproduce the values in the exercise text.

3.3. Solar Ca^+K versus $H\alpha$: line strength

Studying the spectrum of the sun reveals that the Ca^+K line is much stronger than the $H\alpha$ line. Even if the ratio between Calcium and hydrogen abundance in the sun is $2 * 10^6$, and the temperature in the photsphere and chromosphere is $4000 - 6000$ K, the lower ionization energy for Calcium has the potential to excite many more electrons than the Hydrogen.

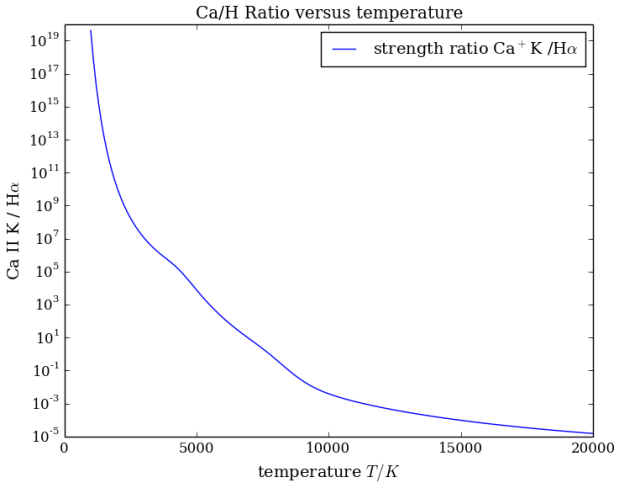

Fig. 4. Calcium hydrogen ratio as a function of temperature.

To prove this I rewrite the function for Schadeenium and use the ionization energies for Calcium instead. We then plot the ratio between the two lines as a function of temperature. See figure 4. Looking at the plot reveals that lower temperature gives higher strength to Calcium. Which makes sense considering the above. As the temperature increases we get enough energy to ionize more and more hydrogen, which makes that stronger than Calcium, since levels 2 and above for Calcium need more energy than the first one for hydrogen. Printing out the ratio at $T = 5000$K gives a ratio of 7643. This doesn't match the value given in the exercise text perfectly but it is close enough to be considered correct.

3.4. Solar Ca^+K versus $H\alpha$: temperature sensitivity

The two lines also differ much in their temperature sensitivity in this formation regime. This can be shown by plotting the relative changes $(\Delta n_{Ca}/\Delta T))/n_{Ca}$ and $(\Delta n_H/n_H)$ for the two lower levels as function of temperature for a small change in temperature ΔT. See figure 5 for a plot of this. Studying the plot we see two dips, one for Ca^+K around $T = 5600$K, and one for $H\alpha$ around $T = 9500$K. From this we can also see that the left side of each dip has $\Delta n < 0$, while the right side has $\Delta n > 0$. To take a closer look at the dips we plot the variation with temperature of each population in relative units on top of the last figure, resulting in figure 6. We see that the relative population for Calcium starts increasing from the start which we expect from its lower ionization energy. After a while all of the Calcium is ionized, and after a bit more we start ionizing the next level and thus the population of this level starts falling. The same mechanism works on hydrogen, but it doesnt fall as fast because of its higher ionization energy. From this it is clear that since the populations remain almost constant for some range of temperatures, the change in the population has to shrink drastically during this range, and that is exactly what we're seeing in the plot. (The dips are right below the tops of the other curves.)

3.5. Hot stars versus cool stars

Finally for this section we want to know what temperature corresponds to about 50% ionization for stellar photospheres with $P_e = 10^2$. To find this we plot the neutral hydrogen fraction

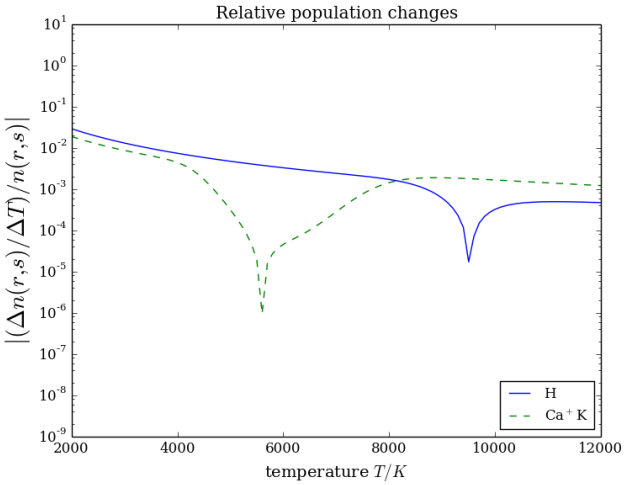

Fig. 5. Relative population change vs temperature.

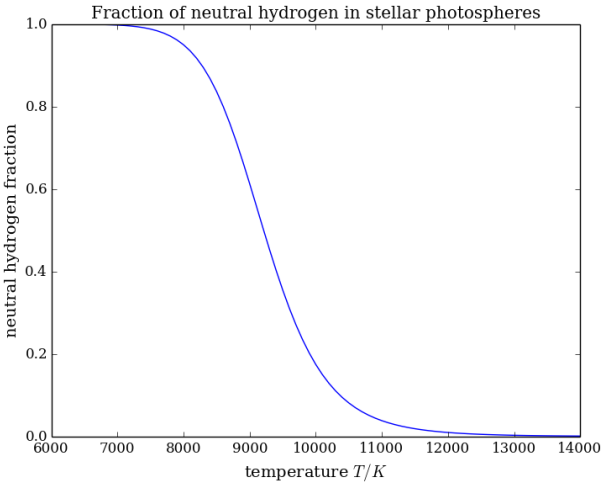

Fig. 7. Neutral hydrogen fraction versus temperature.

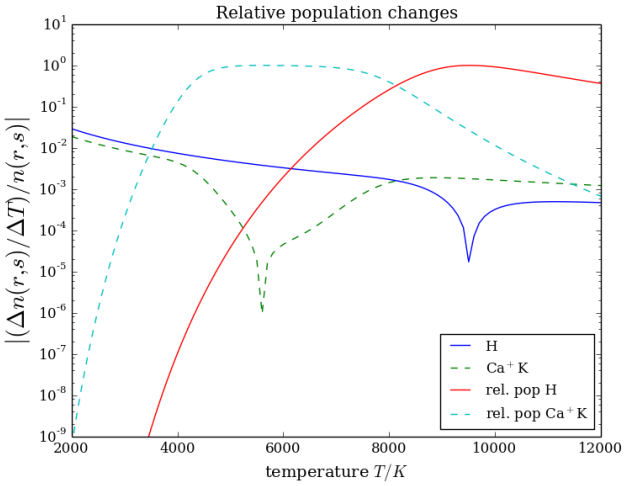

Fig. 6. Relative population change vs temperature in relative units.

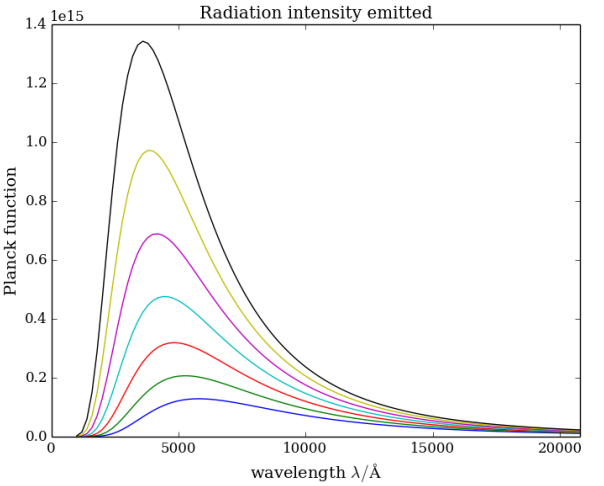

Fig. 8. Planck function for the visible spectrum using different temperatures.

versus temperature and get figure 7, where it looks to be about $9200K$.

4. Fraunhofer line strengths and the curve of growth

4.1. The Planck law

The Planck law is the counterpart to the Saha and Boltzmann distributions for radiation. It specifies the radiation intensity emitted by a gas or body in thermal equilibrium. This is known as a black body. The function is defined

$$B_\lambda(T) = \frac{2hc^2}{\lambda^5}\frac{1}{e^{hc/\lambda kT}-1} \tag{4}$$

We plot this for the visible spectrum for some temperatures in figure 8. We see that the top shifts to lower wavelengths for higher temperatures. We also see that the left side follows the Wien approximation, while the right side follow the Rayleigh-Jeans approximation. The same plot with a logarithmic scale on the y axis can be seen in figure 9, and the same plot with both axes logarithmic can be seen in figure 10. Here we can see even clearer that the Rayleigh-Jeans approximation is correct.

4.2. Radiation through an isothermal layer

It can be shown that the total emergent radiation from a layer with optical thickness $\tau(x)$ and temperature $T(x)$ is:

$$I_\lambda = I_\lambda(0)e^{-\tau} + \int_0^\tau B_\lambda[T(x)]e^{-(\tau-\tau(x))}d\tau(x) \tag{5}$$

If one assumes that the layer is isothermal, this implies that the optical thickness and temperature is independent of position inside the layer. Inserting this into equation 5 gives the following

$$\begin{aligned} I_\lambda &= I_\lambda(0)e^{-\tau} + \int_0^\tau B_\lambda[T(x)]e^{-(\tau-\tau(x)')}d\tau(x)' \\ &= I_\lambda(0)e^{-\tau} + B_\lambda(T)e^{-\tau}\int_0^\tau e^{\tau'}d\tau' \\ &= I_\lambda(0)e^{-\tau} + B_\lambda(T)e^{-\tau}(e^\tau - 1) \end{aligned}$$

$$I_\lambda = I_\lambda(0)e^{-\tau} + B_\lambda(1-e^{-\tau}) \tag{6}$$

Now if we plot this function for $\tau = [0.01, 10]$ with $B = 2$, and $I_\lambda(0) = [0, 4]$ we get figure 11, and if we make the axes logarthimic we get figure 12.

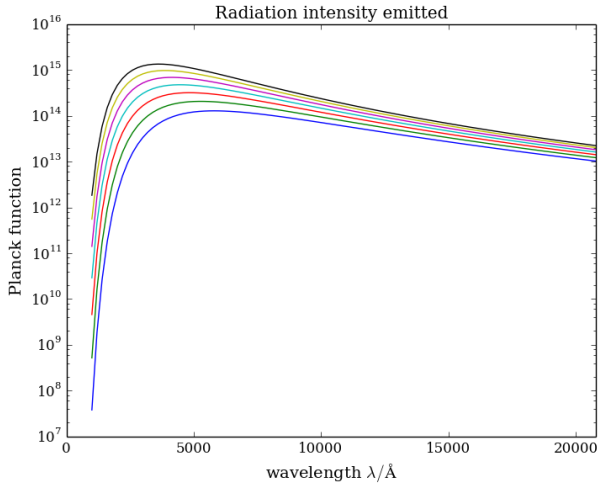

Fig. 9. Logarithimic y axis.

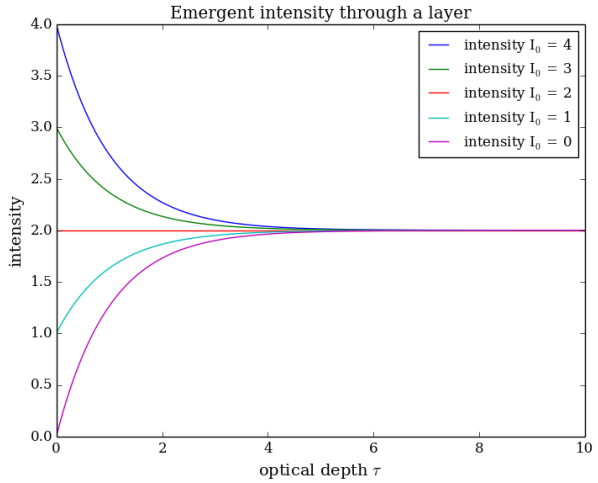

Fig. 11. As the optical depth increases, the intensity converges to the intensity of the Source function B.

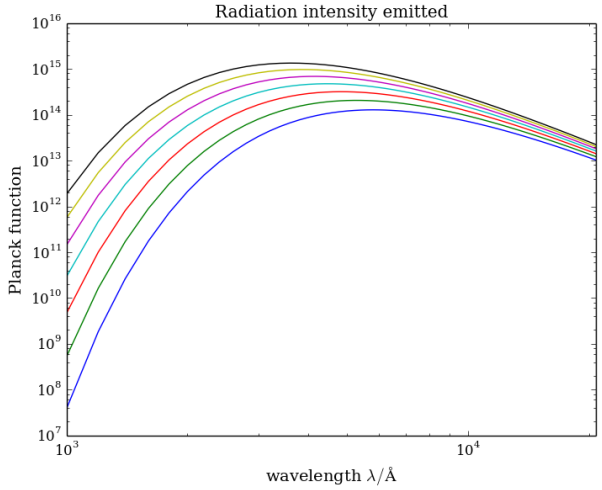

Fig. 10. Both axes logarithmic.

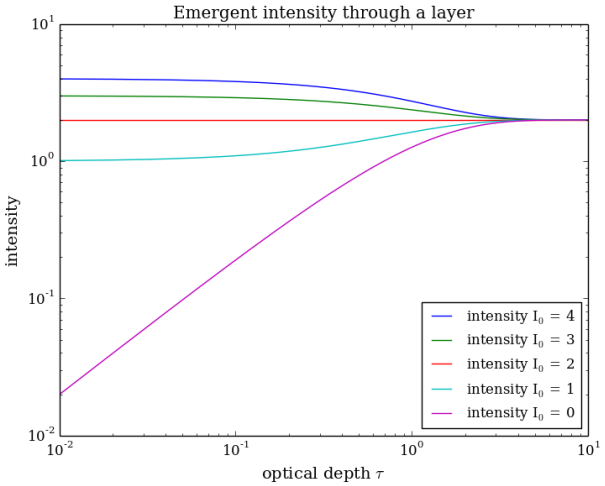

Fig. 12. The emergent intensity with a logarithimic scale.

Studying figures 11 & 12 shows a few different things. If one first considers cases where $\tau << 1$, the figures show that if $I_\lambda(0) = 0$, you get an exponential growth due to the source function B. And if $I_\lambda(0) > B_\lambda$ the intensity stays close to constant. This case corresponds to an "optically thin" medium. This is because whatever intensity that enters the medium passes straight through without being affected by the medium.

The opposite case where $\tau >> 1$ is called an "optically" thick medium, since all the incident radiation is absorbed before it is able to pass through, and is replaced by the radiation emitted by the medium itself. As seen in the plot, the emergent intensity becomes independent of optical depth for large τ. Mathematically this can be seen by looking at equation 6 and letting $\tau \to \infty$. In physical terms one can picture it such that both the incident radiation and the radiation emitted by the medium is absorbed while it is passing through the medium, but since the medium replenishes the radiation it is emitting along the path through it, this radiation is refilled as one goes through the medium,while the incident radiation "runs out" after some distance.

From this it should be clear that optically thin mediums allow us to view radiation originating from the other side of the medium, while optically thick mediums absorb all of the incident radiation before it can pass through, thus blocking our view past them.

4.3. Spectral lines from a solar reversing layer

At this point we choose to use the Schuster-Schwarzschild model. Another name for this model is a reversing-layer model. This model works on the assumption that the continous radiation, without spectral lines, is emitted by the surface of the star, and this radiation then irradiates a seperate layer around the star. This layer is then hit by an intensity

$$I_\lambda(0) = B_\lambda(T_{surface}). \tag{7}$$

This causes emission only at the wavelengths of spectral lines. Next, ones assumes that the star is optically thick, so that the surfrace radiates with the solution of equation 6 where $\tau << 1$, meaning $I_\lambda = B_\lambda(T_{surface})$. This does not mean that shell has to be optically thick. The line-causing atoms in the shell have their own temperature T_{layer}, giving a local production of radiation in the layer for the line-wavelength $B_\lambda(T_{layer})\Delta\tau(x)$. Combining equation 6 & 4.3 yields

$$I_\lambda = B_\lambda(T_{surface})e^{-\tau_\lambda} + B_\lambda(T_{layer})(1 - e^{-\tau_\lambda}) \tag{8}$$

Note that the opaqueness τ in equation 4.3 has gotten an index for wavelength, since it depends on wavelength.

4.3.1. Voigt function

In reality spectral lines are not infinitely sharp delta functions. This can be attributed to Doppler shifts and Coloumb interactions between neighbouring particles. (Even if one could get rid of those effects, you would still have the uncertainty principle spreading it out a little.)

This broadening of the spectral line is described by the distribution

$$\tau(u) = \tau(0)V(a,u) \tag{9}$$

where V is the Voigt function, and u describes the the wavelength separation from the center of the line such that

$$u \equiv \Delta\lambda/\Delta\lambda_D \tag{10}$$

where

$$\Delta\lambda_D \equiv \frac{\lambda}{c}\sqrt{2kT/m}. \tag{11}$$

Here m is the mass of the line-causing particles. The a parameter measures the Coloumb disturbances. For stellar atomspheres a is usually somewhere in the range $[0.01, 0.5]$. The definition of the Voigt function is

$$V(a,u) = \frac{1}{\Delta\lambda_D\sqrt{\pi}}\frac{a}{\pi}\int_{-\infty}^{+\infty}\frac{e^{-y^2}}{(u-y)^2+a^2}dy \tag{12}$$

The Voigt profile represents the convolution(smearing) of a Gauss profile using a Lorentz profile. Because of this it has a Gaussian shape close to line center, and Lorentzian wings on the edges. This can be approximated by taking the sum instead of the convolution giving

$$V(a,u) = \frac{1}{\Delta\lambda_D\sqrt{\pi}}\left[e^{-u^2} + \frac{a}{\sqrt{\pi}u^2}\right] \tag{13}$$

For those using IDL to do calculations, the Voigt function is ready for use through the appropriately named function voigt. Since I use python we instead have to use the fact that the voigt function can be written

$$V(x;\sigma,\gamma) = \frac{Re[w(z)]}{\sigma\sqrt{2\pi}} \tag{14}$$

where Re[w(z)] is the real part of the Faddeeva function evaluated for

$$z = \frac{x+i\gamma}{\sqrt{2}\sigma}\ ,\ a = \frac{\sigma}{\sqrt{2}\sigma}\ ,\ u = \frac{x}{\sqrt{2}\sigma}.$$

In this case the factor $\Delta\lambda_D = \sqrt{2}\sigma$. Luckily for us the Faddeeva function can be found in the special module of the scipy package for python, so that is what we will be using. If we plot this function for different values of a for $u = [-10, 10]$ we get figure 13. To study this we plot the same, but this time with a logarthimic scale for the y axis. The plot can be seen in figure 14. Using approximation 4.3.1 it is clear that the the exponential term vanishes very quickly as $|u|$ increases, leaving us with

$$V(a,u) \approx \frac{a}{\Delta\lambda_D\pi u^2}$$

which gives the functions the same form on the wings just scaled by the factor a.

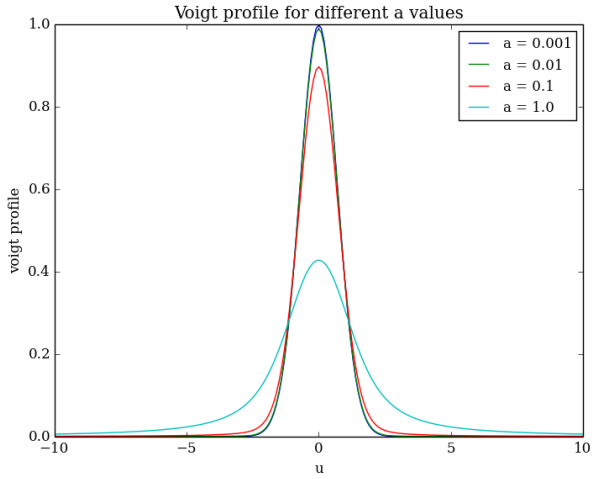

Fig. 13. Voigt profile for different values of a.

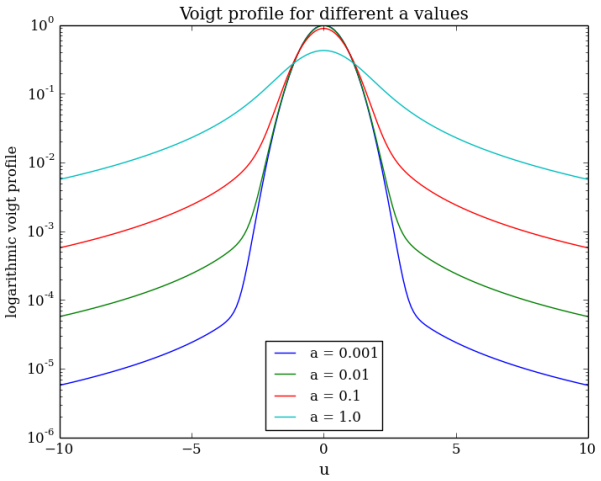

Fig. 14. Logarithmic voigt profile for different values of a.

4.3.2. Emergent line profiles

We now have both functions for intensity and for the distribution of the optical depth. By combining equation 6 & 4.3.1 we should be able to compute and plot stellar spectral line profiles! To do this we use values that fit well with the solar photosphere and plot what it looks like in the visible spectrum. The values we will be using are $T_{surface} = 5700K$, $T_{layer} = 4200K$, $a = 0.01$, $\lambda = 5000$Å. We start by plotting the intensity against u for $\tau(0) = 1$. This results in figure 15.

Next we study the behaviour of the line for $\tau(0)$ in the range $\log\tau(0) = [-2, 2]$. This results in figure 16. Studying this plot reveals that $\tau(0) << 1$ lose almost none of their intensity, just as expected for optically thin media. We also see the "refilling" behaviour of the source function which keeps the saturation above a minimum level. Note also the line wiwngs developing for large $\tau(0)$. This can be attributed to the fact that the intensity is dependent on τ which is dependent on $\tau(0)$ and $V(a,u)$. So the larger $\tau(0)$ is, the longer the exponential terms in equation 4.3 can reduce the intensity. In fact these "wings" don't really converge to the continuum until $u \to \pm\infty$. We can also see from this plot wether the medium is optically thin or thick by recalling that we separate the domains of thickness at the point where the emer-

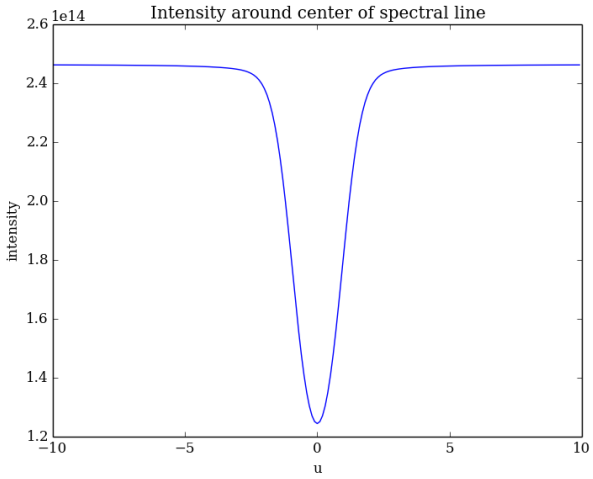

Fig. 15. Spectral lines for wavelength 5000 Å.

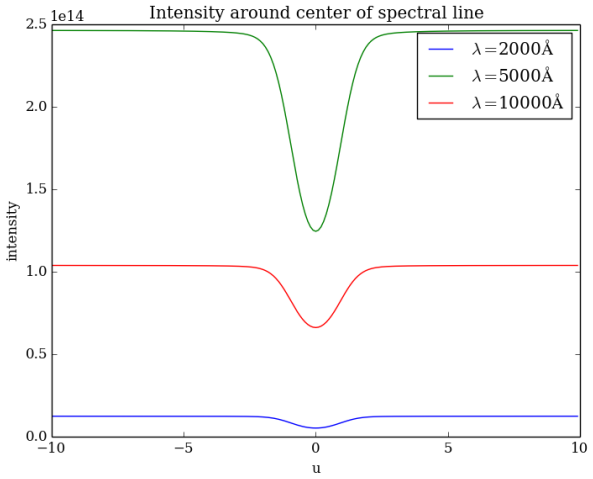

Fig. 17. Spectral lines for different wavelengths.

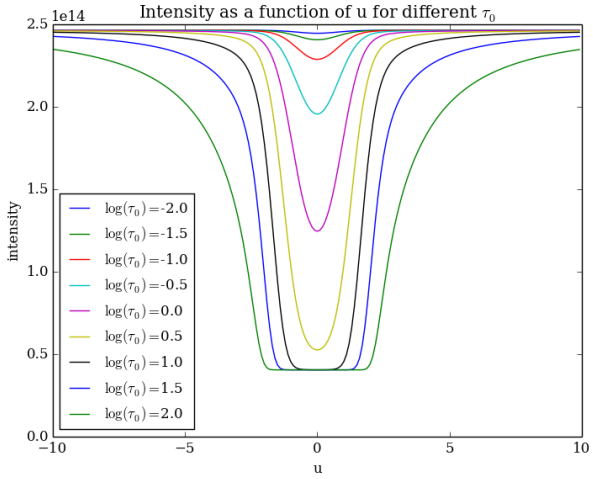

Fig. 16. Spectral lines for different choices of $\tau(0)$ at λ = 5000Å.

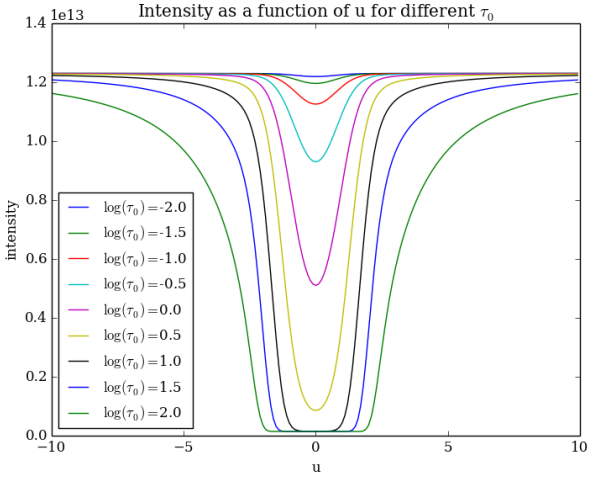

Fig. 18. Spectral lines for different choices of $\tau(0)$ at λ = 2000Å.

λ	I_{cont}	I_{center}
2000	1.23×10^{13}	1.36×10^{11}
5000	2.46×10^{14}	4.04×10^{13}
10000	1.04×10^{14}	4.00×10^{13}

Table 1. Intensity of the continuum

gent radiation has been reduced to a factor $1/e$ of its incident radiation. In this case we see from the plot that the incident radiation is about 2.5×10^{14} so anything below about $0.9 \times 10^{1}4$ is optically thick, while anything above is optically thin. Thus we see that from the plot that in this case we get an optically thick medium if $\log \tau(0) = 0$ or less. Strictly speaking the limit is somwhere between this and $\log \tau(0) = 0.5$. If we shift our view to the sides of the line center to e.g $u = 5$ all of the plotted lines are well above the limit for optically thin.

Looking at the spectral lines for different wavelengths reveal a difference in intensity. This can be seen in figure 17. To check the behaviour for different wavelengths we plot the results for λ = 2000 & 10000 in figures 18 & 19.

For the two other wavelengths we see the same behaviour as we did for λ = 5000Å. The shapes are the same, while the intensity of the continuum changes. The lower limit also moves. For λ = 2000Å we end up with a separation between optically thin and thick at roughly the same place as for λ = 5000Å. However, for λ = 10000Å the intensity reaches the lower limit before it can be reduced to the point where we say the medium is optically thick. This would indicate that the medium is optically thin at very high wavelengths. To find the value of the continuum we look at the equation for the emergent intensity (eq. 4.3). To look at the continuum we set $\tau \to 0$, since the continuum should have no optical depth. This gives

$$I_{cont} = B_\lambda(T_{surface}) \tag{15}$$

so the intensity of the continuum is defined by the surface temperature. While if we let $\tau \to \infty$ we get the lower limit

$$I_{min} = B_\lambda(T_{layer}) \tag{16}$$

We check these values by printing them to the commandline in our function. The results of this can be found in table 4.3.2. Calculating them from the Planck function gives the same answers. Since some observed spectra are measured without absolute intensity calibration it is useful to scale the spectrum to the local continuum intensity by plotting I_λ / I_{cont}. Plotting this for the same 3 wavelengths reults in figure 20.

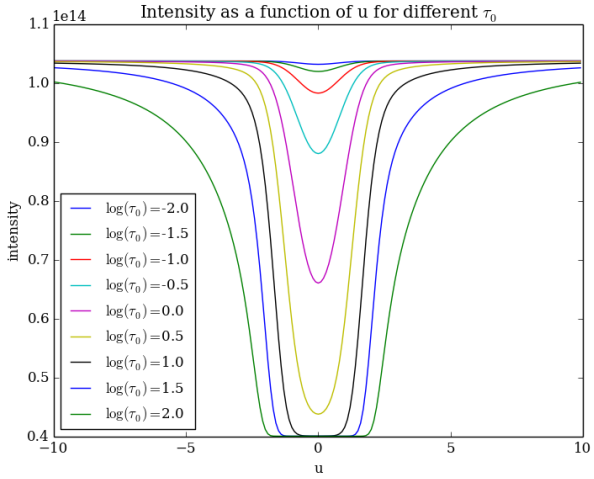

Fig. 19. Spectral lines for different choices of $\tau(0)$ at $\lambda = 10000$Å.

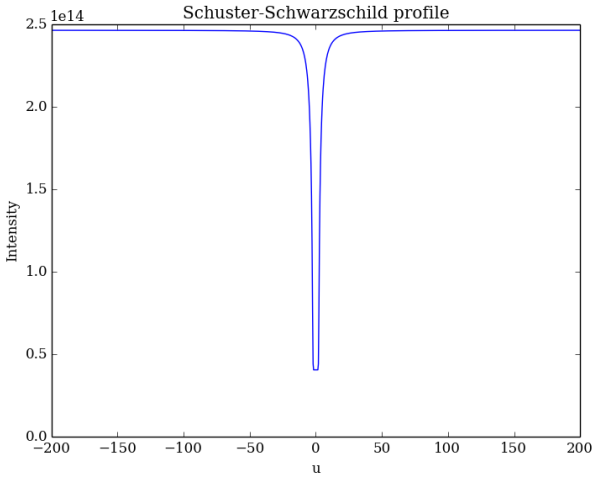

Fig. 21. Schuster-Schwarzschild profile.

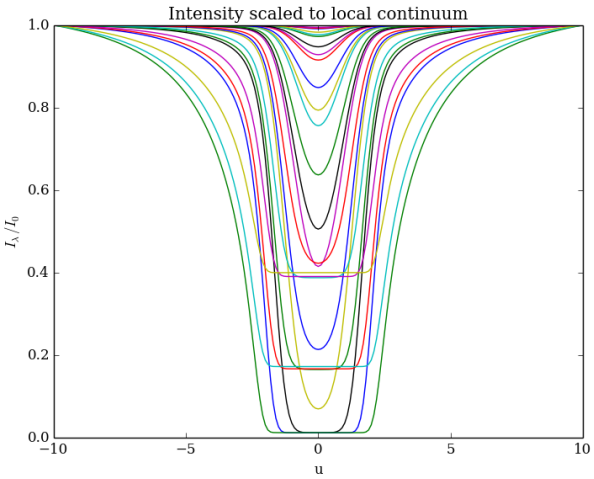

Fig. 20. Spectral lines for different choices of $\tau(0)$.

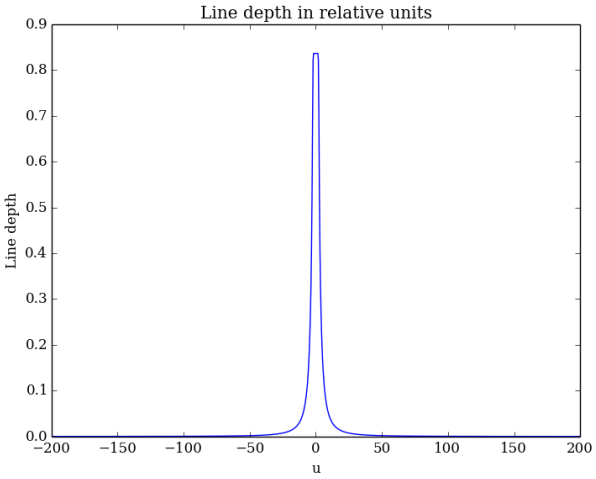

Fig. 22. Line depth in relative units.

4.4. The equivalent width of spectral lines

From the profile plots one can see that the growth of the absorption feature for increasing $\tau(0)$is faster for small $\tau(0)$ than for larger $\tau(0)$. Because of this, Minnaert and his coworkers introduced the equivalent width W_λ as a line-strength parameter to measure this effect. It measures the integrated line depression in the normalized spectrum

$$W_\lambda = \int \frac{I_{cont} - I(\lambda)}{I_{cont}} d\lambda. \tag{17}$$

To test this effectively we make a profile function that returns a Schuster-Schwarzschild profile, given a, τ, and u. Setting $a = 0.1$, $\tau(0) = 100$ and plotting this for $u = [-200, 200]$ returns figure 21.

Next we compute the line depth in relative units(the integrand in equation 4.4. Plotting this versus u gives figure 22.

In this test case we get an equivalent width $W_\lambda = 7.5$.

4.5. The curve of growth

The point of the equivalent width was that it could be used to measure the number of atoms in the reversing layer. This should set the opaqueness $\tau(0)$ of the layer. The profile plots show that the profile growth is only linear with $\tau(0)$ for $\tau(0) << 1$. The curve of growth shows the full dependence; the growth of the line strength with the line-causing density.

To study this we plot log W_λ against log $\tau(0)$ in figure 23.

- Explain what happens in the three different parts
- The first part has slope 1:1 ,the third has slope 1:2 in this log-log plot. Why?
- Which parameter controls the location of the onset of the third part? Give a rough estimate of its value for solar iron-lines through comparison with figure 14 in the assignment.
- Final: of which parameter should you raise the numerical value in order to produce emission lines instead of absorption lines? Change it accordingly and rerun your programs to produce emission profiles and an emission-line curve of growth. Avoid plotting negative W_λ values logarithimically by plotting the absoulte value of equivalent width.

5. Conclusions

insert conclusions

Acknowledgements.

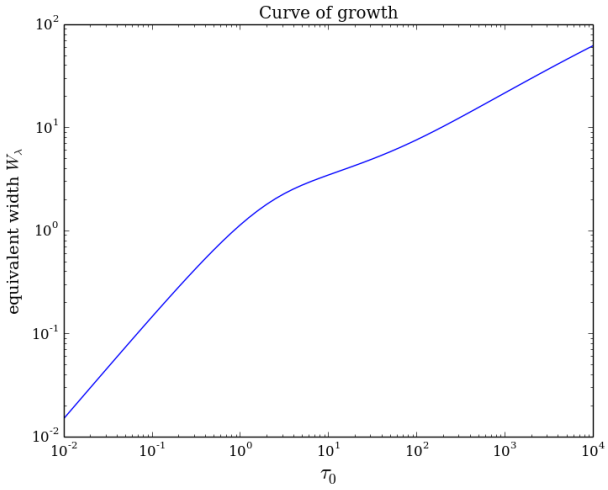

Fig. 23. Curve of Growth.